Reprinted from

Applied Physics Letters

Volume 64 30 May 1994 Number 22

Very long-wavelength GaAs/$Al_xGa_{1-x}As$ infrared hot electron transistor

S. D. Gunapala, J. S. Park, T. L. Lin, and J. K. Liu
Center for Space Microelectronics Technology, Jet Propulsion Laboratory, California Institute of Technology, Pasadena, California 91109

K. M. S. V. Bandara
Department of Physics, University of Peradeniya, Peradeniya, Sri Lanka

(Received 14 January 1994; accepted for publication 14 March 1994)

pp. 3003-3005

a publication of the American Institute of Physics

Very long-wavelength GaAs/$Al_xGa_{1-x}As$ infrared hot electron transistor

S. D. Gunapala, J. S. Park, T. L. Lin, and J. K. Liu
Center for Space Microelectronics Technology, Jet Propulsion Laboratory, California Institute of Technology, Pasadena, California 91109

K. M. S. V. Bandara
Department of Physics, University of Peradeniya, Peradeniya, Sri Lanka

(Received 14 January 1994; accepted for publication 14 March 1994)

We have demonstrated a bound-to-continuum state GaAs/$Al_xGa_{1-x}As$ infrared hot electron transistor which has a peak response at $\lambda_p=16.3$ μm. This device utilizes a bound-to-continuum quantum well infrared photodetector as a photosensitive emitter and a wide $Al_xGa_{1-x}As$ barrier between the base and the collector as an energy discriminating filter. An excellent photocurrent transfer ratio of $\alpha_p=0.12$ and very low dark current transfer ratio of $\alpha_d=7.2\times10^{-5}$ is achieved at a temperature of $T=60$ K.

Infrared (IR) detectors and imaging systems that operate in the wavelength range 3–18 μm are required in many space applications such as monitoring the global atmospheric temperature profiles, relative humidity profiles, cloud characteristics, and the distribution of minor constituents in the atmosphere which are being planned for the NASA's Earth Observing System (EOS). These space applications have placed stringent requirements on the performance of the IR detectors and arrays including high detectivity, low dark current, radiation hardness, and lower power dissipation. Also this spectral region is rich in information vital to the understanding of composition, structure, and the energy balance of molecular clouds and star forming regions of our galaxy. Thus there is a great interest in IR detectors operating both inside and outside the atmospheric windows (3–5 μm and 8–12 μm).

Since the GaAs based quantum well infrared photodetectors (QWIPs)[1] which utilize the intersubband transitions meet most of the above-mentioned requirements, these detectors should be very attractive for the detection of IR radiation in the 6–18 μm spectral range. However, the only problem associated with the very long wavelength QWIPs ($\lambda>12$ μm) is the higher dark current which adversely affects detector performance. By analyzing the dark current of shallow quantum wells which were designed for very long wavelength operation, we have realized that at low temperatures (<60 K) the total tunneling contribution of the dark current (sequential tunneling+thermionic assisted tunneling) is significantly higher than the thermionic contribution of the dark current (Fig. 1). The conduction electrons carrying these two tunneling current components are lower in energy than the photoelectrons.[2] Thus an IR hot electron transistor (IHET),[3–5] which has an additional wide $Al_xGa_{1-x}As$ barrier to filter out sequential tunneling and thermionic assisted tunneling currents, will perform better at very long wavelength than QWIP.

In order to analyze the dark current of a QWIP which has a intersubband absorption peak at 16 μm, we first calculated the effective number of electrons[6,7] $n(V)$ which are thermally excited into the continuum transport states, as a function of bias voltage V, using the following expression.

$$n(V)=\left(\frac{m^*}{\pi\hbar^2 L_p}\right)\int_{E_0}^{\infty} f(E)T(E,V)\,dE. \tag{1}$$

The first factor containing the effective mass m^* represents the average three-dimensional density of states. Where L_p is the superlattice period, $f(E)$ is the Fermi factor $f(E)=[1+\exp(E-E_0-E_F)/KT]^{-1}$, E_0 is the bound state energy, E_F is the two-dimensional Fermi energy, E is the energy of the electron, and $T(E,V)$ is the tunneling current transmission factor which is obtained by using Wentzel–Kramers–Brillouin (WKB) approximation to a biased quantum well. In Eq. (1), the effective number of electrons above the barrier account for thermionic contribution and the number of electrons below the barrier account for thermionic assisted tunneling and tunneling contribution of the dark current. Then the bias-dependent dark current $I_d(V)$ was calculated, using $I_d(V)=eAn(V)v(V)$, where $v(V)$ is the average transport velocity, A is the device area, and e is the electronic charge. The average transport velocity was calculated using $v(V)=\mu F[1+(\mu F/v_s)^2]^{-1/2}$, where μ is the mobility, F is the electric field, and v_s is the saturated drift velocity.[8] In order to obtain $T=60$ K, bias-dependent dark current $\mu=1200$ $cm^2/V\,s$ and $v_s=5.5\times10^6$ cm/s was used. Figure 1 shows the $T=60$ K dark current due to thermionic emission, total dark current (thermionic+thermionic assisted tunneling+tunneling), and experimental dark current of a QWIP sample which has wavelength cutoff $\lambda_c=17.8$ μm. According to the calculations tunneling through the barriers dominate the dark current at temperature below 30 K, at temperatures between 30–55 K thermionic assisted tunneling might become important, and at temperatures above 55 K thermionic emission into the continuum transport states dominate the dark current.

As shown in Fig. 2 the device structure consisted of a multiquantum well region of 50 periods of 500-Å undoped $Al_{0.11}Ga_{0.89}As$ barrier and 65-Å doped GaAs well. The quantum wells were doped to $n=5\times10^{17}$ cm^{-3}, and sandwiched between a heavily doped ($n=1\times10^{18}$ cm^{-3}) 1-μm GaAs contact layer at the bottom as the emitter contact and a doped ($n=3\times10^{17}$ cm^{-3}) 500-Å GaAs layer on the top as the base contact. On top of the base a 2000-Å undoped $Al_{0.11}Ga_{0.89}As$ layer and a doped ($n=3\times10^{17}$ cm^{-3}) 0.5-μm GaAs layer

 0003-6951/94/64(22)/3003/3/$6.00

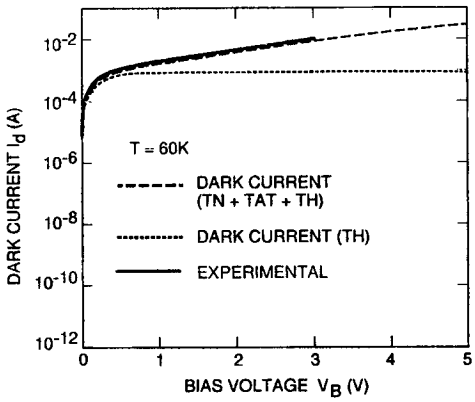

FIG. 1. Theoretical and experimental (solid) dark current-voltage curves at $T=60$ K. Dotted curve shows the dark current (theoretical) due to thermionic emission only. Dashed curve shows the total dark current (thermionic +tunneling+thermionic assisted) vs bias voltage.

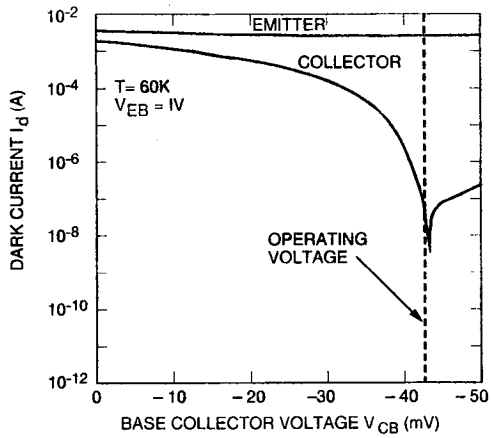

FIG. 3. IHET emitter and collector dark currents vs base-collector voltage at $T=60$ K. Emitter bias was kept at -1 V relative to the base potential. This figure also shows the lower energy dark current filtration capability of the quantum filter.

were grown. The 2000-Å undoped $Al_{0.11}Ga_{0.89}As$ As layer acted as a discriminator between the tunnel-electrons and photoelectrons, and the top 0.5-μm GaAs layer served as the collector. This device structure was grown on a semiinsulating GaAs substrate using molecular beam epitaxy. The inset of the Fig. 2 shows the diagram of the device. QWIP operation can be obtained between the emitter and the base and all the terminals (three) are required for the IHET operation. The IHET currents were measured at the collector (low-energy tunneled electrons drain through the base).

To facilitate the application of bias to the quantum well structure, the following processing steps were carried out. First, arrays of 200×200 μm^2 square collectors were chemically etched. In the next processing step the 6.25×10^{-4} cm^2 QWIP mesas which overlap with collector mesas were etched. Finally, Au/Ge ohmic contacts were evaporated onto the emitter, base, and collector contact layers. The emitter and collector dark currents versus base-collector bias voltage are shown in Fig. 3. This figure also shows the excellent dark current filtration capability of the quantum filter. The dark current transfer ratio ($\alpha_d=I_{C(\text{dark})}/I_{E(\text{dark})}$) is 7.2×10^{-5} at operating base-collector bias voltage $V_{CB}=-42$ mV (Fig. 3).

The intersubband absorption was measured on a 45° polished multipass waveguide[1] at $T=60$ K and absorption coefficient $\alpha=694$ cm^{-1} at $\lambda_p=17.1$ μm was obtained. This α corresponds to an unpolarized absorption quantum efficiency $\eta=(1-e^{-2\alpha l})/2=16.5\%$.[1,9] Also these 200×200 μm^2 square detectors were back illuminated through a 45° polished facet as previously described in detail[1] and responsivity spectrums were measured with a tunable source consisting of a 1000 K blackbody and a grating monochromator. The emitter and collector responsivity spectrums measured at $T=60$ K are shown in Fig. 4. These two spectrums are similar in shape and peak at $\lambda_p=16.3$ μm. The values of the cutoff wavelength λ_c and the spectral width ($\Delta\lambda/\lambda$) (full width at half-maximum) are 17.3 μm and 20%, respectively. The absolute responsivity was measured by two different methods; by comparing the detector photoresponse with the photoresponse of a calibrated pyroelectric detector, and by using a calibrated blackbody source. The peak responsivity R_p of the detector was 400 mA/W. Figure 5 shows the IHET emitter and collector photocurrents versus base-collector voltage at $T=60$ K. The emitter was kept at -1-V bias relative to the

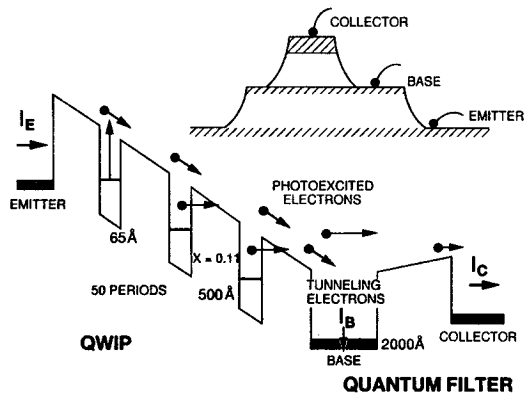

FIG. 2. Conduction-band diagram of a infrared hot electron transistor, which utilizes bound-to-continuum intersubband transition. The inset shows the schematic diagram of IHET.

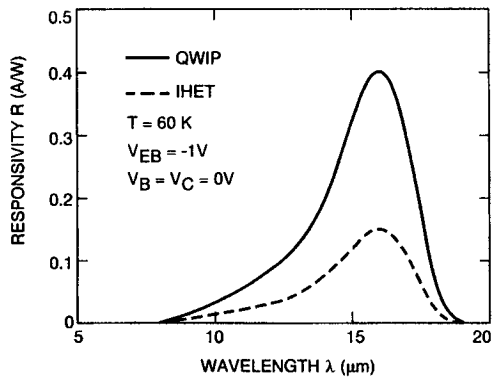

FIG. 4. Emitter and collector responsivity spectra at temperature $T=60$ K. Emitter was kept at -1-V bias relative to the base and collector.

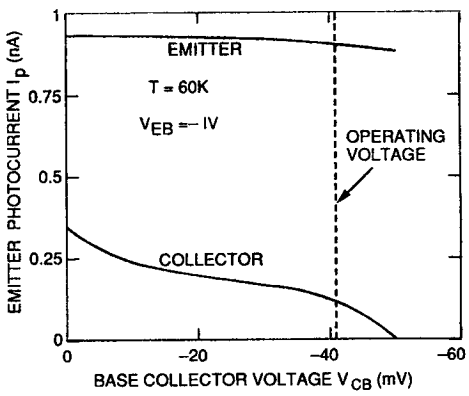

FIG. 5. IHET emitter and collector photocurrents vs base-collector voltage at $T=60$ K. Emitter was kept at −1-V bias relative to the base potential.

base potential. Due to the hot electron relaxation in the wide base region, the photocurrent at the collector is smaller relative to the emitter photocurrent. The photocurrent transfer ratio ($\alpha_p = I_{C(\text{photo})}/I_{E(\text{photo})}$) is 1.2×10^{-1} at $V_{CB}=-42$ mV. Note that the α_d is more than three orders of magnitude smaller than α_p which clearly indicates that the dark current of IHET is four orders of magnitude smaller than the dark current of QWIP, while the photocurrent is reduced by an order of magnitude only. This four orders of magnitude reduction in dark current reduces the noise current by two orders of magnitude (and hence, results in higher detectivity).

The optical gain g of the detector determined from $R=(e/h\nu)\eta g$ is given by $g=0.2$. The noise current[1] i_n was calculated using $i_n=\sqrt{4eI_dg\Delta f}$, where Δf is the bandwidth. The calculated noise current of the detector is $i_n=17$ pA at $T=60$ K. The peak D^* can now be calculated from $D^*=R\sqrt{A\Delta f}/i_n$. The calculated D^* between the emitter and the base (QWIP) at $V_{EB}=-1$ V, $V_{CB}=-42$ mV, and $T=60$ K is 5.8×10^8 cm$\sqrt{\text{Hz}}$/W. The detectivity D^* at the collector (IHET) is determined[4] from D^* (IHET)$=(\alpha_p/\sqrt{\alpha_d})$ D^* (QWIP). Table I shows the QWIP and IHET detectivity D^* at temperature $T=60$ K for several base-collector bias voltages. As shown in Table I the D^* of IHET is higher than the D^* of two terminal multiquantum well detectors, due to the low-energy dark current filtering effect.

TABLE I. Comparison of QWIP and IHET detectivity D^* at temperature $T=60$ K for several base-collector bias voltages.

V_{BC} (mV)	α_p/α_d	D^*_{QWIP} ($10^8\times$cm$\sqrt{\text{Hz}}$/W)	D^*_{IHET} ($10^8\times$cm$\sqrt{\text{Hz}}$/W)
−30	0.72	6.0	4.3
−35	1.17	5.9	6.9
−40	3.98	5.9	23
−42	14.14	5.8	82

In summary, we have demonstrated a very long wavelength ($\lambda_c=17.3$ μm) IHET. Even though the QWIP emitters we have used were not optimized for 16-μm operation, this device clearly shows the dark current filtration capability of the energy filter. Thus by incorporating an energy discriminating filter to an optimized QWIP with random reflector[10] which operates at 16 μm ($D^*=5\times10^{10}$ cm$\sqrt{\text{Hz}}$/W at $T=60$ K), it is possible to achieve a detectivity of 1×10^{11} cm$\sqrt{\text{Hz}}$/W at $T=60$ K. In fact, by utilizing random reflectors (increase quantum efficiency) and reducing the well doping density (reduce thermal generation rate), performance of QWIPs and IHETs can be made close to that of HgCdTe detectors.[11] In addition, due to excellent uniformity, radiation hardness, lower power dissipation, lower $1/f$ noise,[1] and large R_0A product these GaAs based QWIPs and IHETs should be extremely attractive for space-borne applications such as EOS missions and IR astronomy.

We are grateful to K. K. Choi of the Army Research Laboratory and B. F. Levine of the AT&T Bell Laboratories for many useful discussions, and C. A. Kukkonen, V. Sarohia, S. Khanna, K. M. Koliwad, and B. A. Wilson of the Jet Propulsion Laboratory for encouragement and support of this work. The research described in this letter was performed by the Center for Space Microelectronics Technology, Jet Propulsion Laboratory, California Institute of Technology, and was jointly sponsored by the Ballistic Missile Defense Organization/Innovative Science and Technology Office, and the National Aeronautics and Space Administration, Office of Advanced Concepts and Technology.

[1] B. F. Levine, J. Appl. Phys. **74**, R1 (1993).
[2] K. K. Choi, M. Dutta, P. G. Newman, M. L. Saunders, and G. L. Iafrate, Appl. Phys. Lett. **57**, 1348 (1990).
[3] K. K. Choi, M. Dutta, and R. P. Moerkirk, Appl. Phys. Lett. **58**, 1533 (1991).
[4] K. K. Choi, M. Taysing-Lara, L. Fotiadis, and W. Chang, Appl. Phys. Lett. **59**, 1614 (1991).
[5] K. K. Choi, L. Fotiadis, M. Taysing-Lara, and W. Chang, Appl. Phys. Lett. **59**, 3303 (1991).
[6] S. D. Gunapala, B. F. Levine, L. Pfeiffer, and K. West, J. Appl. Phys. **69**, 6517 (1990).
[7] B. F. Levine, C. G. Bethea, G. Hasnain, V. O. Shen, E. Pelve, R. R. Abbott, and S. J. Hsieh, Appl. Phys. Lett. **56**, 851 (1990).
[8] In QWIPs and IHETs most of the tunneling comes from near the top of the barrier (triangular part of the biased barrier) where electrons tunnel into the continuum levels. Equation (1) calculates the density of electrons which have tunneled into the continuum by including $T(E,V)$ term. Well-to-well tunneling contribution can be neglected because it is many orders of magnitude smaller (due to thick barriers) than other dark current components.
[9] Factor 2 in the denominator converts the polarized quantum efficiency into unpolarized quantum efficiency.
[10] G. Sarusi, B. F. Levine, S. J. Pearton, K. M. S. V. Bandara, and R. E. Leibenguth, Appl. Phys. Lett. **64**, 960 (1994).
[11] K. Choi, C. Y. Lee, M. Z. Tidrow, W. H. Chang, and S. D. Gunapala (unpublished).